Plasmonics (2015) 10:667–673
DOI 10.1007/s11468-014-9852-7

The Ag Nanoparticles/TiO_2 Thin Film Device for Enhanced Photoconduction and Role of Traps

A. Mondal · A. Ganguly · A. Das · B. Choudhuri · R. K. Yadav

Received: 20 September 2014 / Accepted: 25 November 2014 / Published online: 6 December 2014

Abstract Glancing angle deposition technique was carried out to synthesize silver (Ag) nanoparticles (NPs) on titanium dioxide (TiO_2) thin film (TF) over n-type Si substrate. The presence of Ag NPs on the TiO_2 TF enhanced the photoconduction as compared to bare TiO_2 TF. The maximum photosensitivity of the Ag NPs/TiO_2 TF (plasmonic) device was recorded ~700 times than that of the bare TiO_2 TF at −3 V. The devices were UV sensitive and maximum internal gain for the plasmonic device was calculated to be ~210 at 380 nm. The inversion capacitance of the plasmonic devices responded with a.c. signal efficiently as compared to bare TiO_2 TF. Under applied sweeping top electrode voltage *V*s ±10 V, the corresponding maximum memory window of 4.5 V was observed for plasmonic device in its capacitance (C)–voltage (V) curve. The Ag NPs-patterned TiO_2 TF device possessed higher impedance than that of the bare TiO_2 TF-based device.

Keywords Glancing angle deposition · Surface plasmon · Silver nanoparticles · TiO_2 thin film

Introduction

Titanium dioxide (TiO_2) is a popular photocatalytic material [1–3] which lacks visible light absorption due to its high optical band gap energy (3.2 eV) [4]. The presence of plasmonic nanoparticles (NPs) such as silver (Ag) can enhance the absorption of TiO_2 in the visible region and therefore, its photocatalytic activity [5]. The presence of metal NPs (Ag NPs) produced localized surface plasmon resonance (LSPRs), which coupled with the medium like TiO_2 to enlarge the optical cross-sections of the LSPRs and increase the optical path length of the incident photons and thus the absorption also [6]. Therefore, the overall backscattering and dissipation of light absorption over short wavelength were suppressed, resulting in an increase in the photocurrent conversion efficiency. Again, the Ag NPs on the TiO_2 thin film (TF) attract the oxygen molecules from the TiO_2 and introduce defect states [7]. The absorption of photon can be enhanced due to the sub band gap transitions of the said material via the defects. The introduced trap states can enhance the photosensitivity of the fabricated device by hole trapping process as discussed elsewhere [8]. Presently, the superior performances of multilayered TiO_2 TF-based memory devices have been investigated by introducing the metal NPs like platinum (Pt) in between two successive layers [9]. The enhanced charge-trapping ability of the devices was related to the interface defects [10–12], which appeared due to the metal NPs into the system. Again, the ability and advantages of glancing angle deposition (GLAD) technique for synthesis of metal NPs like silver (Ag) and indium (In) were discussed by the authors [13, 14]. In this paper, we have synthesized the Ag NPs on the TiO_2 TF by GLAD. The production of enhanced current under illumination condition was examined and discussed elaborately in view of hole trapping process under reverse bias condition. The maximum and enlarged UV light detection by the Ag NPs-patterned TiO_2 TF-based devices were experimented as compared to bare TiO_2 TF. The enhanced charge-trapping capability of Ag NPs/TiO_2 TF/n-Si device was investigated by comparing with that of the TiO_2 TF/n-Si. The low impedance and high dark conductivity of the bare TiO_2 TF was observed as compared to Ag NPs/TiO_2 TF device.

A. Mondal
Department of Physics, National Institute of Technology Durgapur, Durgapur 713209, India

A. Mondal (✉) · A. Das · B. Choudhuri
Department of Electronics and Communication Engineering, National Institute of Technology Agartala, Jirania, Tripura (West) 799046, India
e-mail: aniruddhamo@gmail.com

A. Ganguly · R. K. Yadav
Department of Physics, National Institute of Technology Agartala, Jirania, Tripura (West) 799046, India

Experiments

The GLAD technique has been carried out to synthesize the pure Ag (MTI, USA) NPs on n-type Si <100> substrate coated with 150 nm TiO_2 TF. The substrates were rotated azimuthally with a constant speed of 460 rpm at an orientation of 85 ° with respect to the perpendicular line between the metal source and the planar substrate holder. The depositions were carried out at a base pressure of ~2×10^{-5} mbar inside the e-beam evaporator chamber. A deposition rate of 1.2 Å/s was kept constant. A 50 nm TiO_2 cover layer was then deposited on Ag NPs-patterned TiO_2 TF. Gold (Au) and Ag contacts were made separately as top electrodes (area of ~1.77×10^{-6} m^2) of the fabricated plasmonic devices on the cover layer (50 nm TiO_2 TF).

The current (I)–voltage (V) characteristics of the samples were investigated by using a Keithley 2400 source measure unit through Au electrode. The wavelength-dependent photo responsivity of the detector was measured using 300 W xenon arc lamp (650–0047) through a monochromator (Sciencetech Inc., Canada) in open beam configuration. The capacitance of the Ag NPs/TiO_2 TF-based plasmonic and TiO_2 TF devices were measured by Agilent (E4980A) LCR meter using Ag top contact.

Results and Discussion

Device Conduction

Figure 1a shows the schematic of the bare TiO_2 TF and Ag NPs-patterned TiO_2 TF (plasmonic)-based devices. The top view SEM image of the Ag NPs-patterned TiO_2 TF on n-Si substrate was reported by the authors [14]. Figure 1b shows the I–V characteristics for the TiO_2 TF device and the Ag NPs/TiO_2 TF-based device using Au Schottky contact. The devices were tested under dark and illumination condition.

Under dark condition, the TiO_2 TF-based detector produced large current in the reverse bias mode as compared to Ag NPs/TiO_2 TF-based plasmonic device (Fig. 1b). But under photon illumination from xenon lamp (300 W), the TiO_2 TF was almost unresponsive, whereas the plasmonic detector was highly sensitive under reverse bias. The dark current of the TiO_2 TF at −3 V was 44×10^{-3} mA/cm^2 and for Ag NPs/TiO_2 TF was 7.6×10^{-3} mA/cm^2, which deflected to 55×10^{-3} mA/cm^2 and 3.98 mA/ cm^2, respectively, under illumination. The lower current value of the plasmonic device compared to that of the bare TiO_2 TF device was due to the presence of large trap states into the Ag NPs/TiO_2 TF sample. Again, the photosensitivity of the TiO_2 TF and Ag NPs/TiO_2 TF devices were calculated for both the reverse bias and forward bias conditions from the ratio of light to dark current of the detectors separately. There was no significant enhancement in photosensitivity (Fig. 1c) observed for the Ag NPs/TiO_2 TF device as compared to that of the TiO_2 TF, under the applied potential range 0 to +8 V. But the plasmonic (Ag NPs/TiO_2 TF) device exhibited enlarged photo efficiency under the reverse bias condition when compared with the forward bias. The maximum photosensitivity of the Ag NPs/TiO_2 TF device was ~700 times than that of the TiO_2 TF at −3 V. The coupling of Ag NPs LSPRs and TiO_2 layer enhanced the intensity and optimized the projection of the internal electromagnetic field induced by the metal LSPRs. Therefore, the overall backscattering and dissipation of light absorption over 300–700 nm were suppressed, resulting in an increase in the photocurrent. Also, the Ag NPs produced Ag–O NPs [7], introduced oxygen defect related more trap states into the band gap of TiO_2 material by attracting the oxygen molecules from structurally unstable TiO_2 [15]. Under forward bias, a large number of electron–hole pairs were generated, which were available to ionize (by the scattering process) the interface states at Au/TiO_2 TF and increased the depletion region [16] thus preventing the increase in photosensitivity. However, in case of the reverse bias, the trap states at the metal–semiconductor interface trapped holes [17], which efficiently reduced both the depletion width and the Schottky height at the junction. In addition, the electron–hole pairs were prevented from recombination and the photo-generated electrons became available to conduct the current into the device. Again, the minimum depletion layer width and hence the maximum electron tunneling happened at −3 V applied potential, which resulted in the extreme efficiency of the plasmonic device.

The ideality factor (n) and the Schottky barrier height (SBH) of the TiO_2 TF and Ag NPs/TiO_2 TF-based detectors were evaluated by using the following equation based on the thermionic emission theory [18].

$$I = AA^{**}T^2 e^{\left(\frac{-q\phi_b}{kT}\right)}\left[e^{\left(\frac{-qV}{nkT}\right)}-1\right] \tag{1}$$

$$I = I_0\left[e^{\left(\frac{-qV}{nkT}\right)}-1\right] \text{ for } V > \frac{3kT}{q} \tag{2}$$

Where A is the contact area, V is the applied voltage drop across the rectifying barrier, T is the absolute temperature in Kelvin, K is the Boltzmann constant, q is the charge of an electron, n is the ideality factor, and I_0 is the saturation current given by

$$I_0 = AA^{**}T^2 e^{\left(\frac{-q\phi_b}{kT}\right)} \tag{3}$$

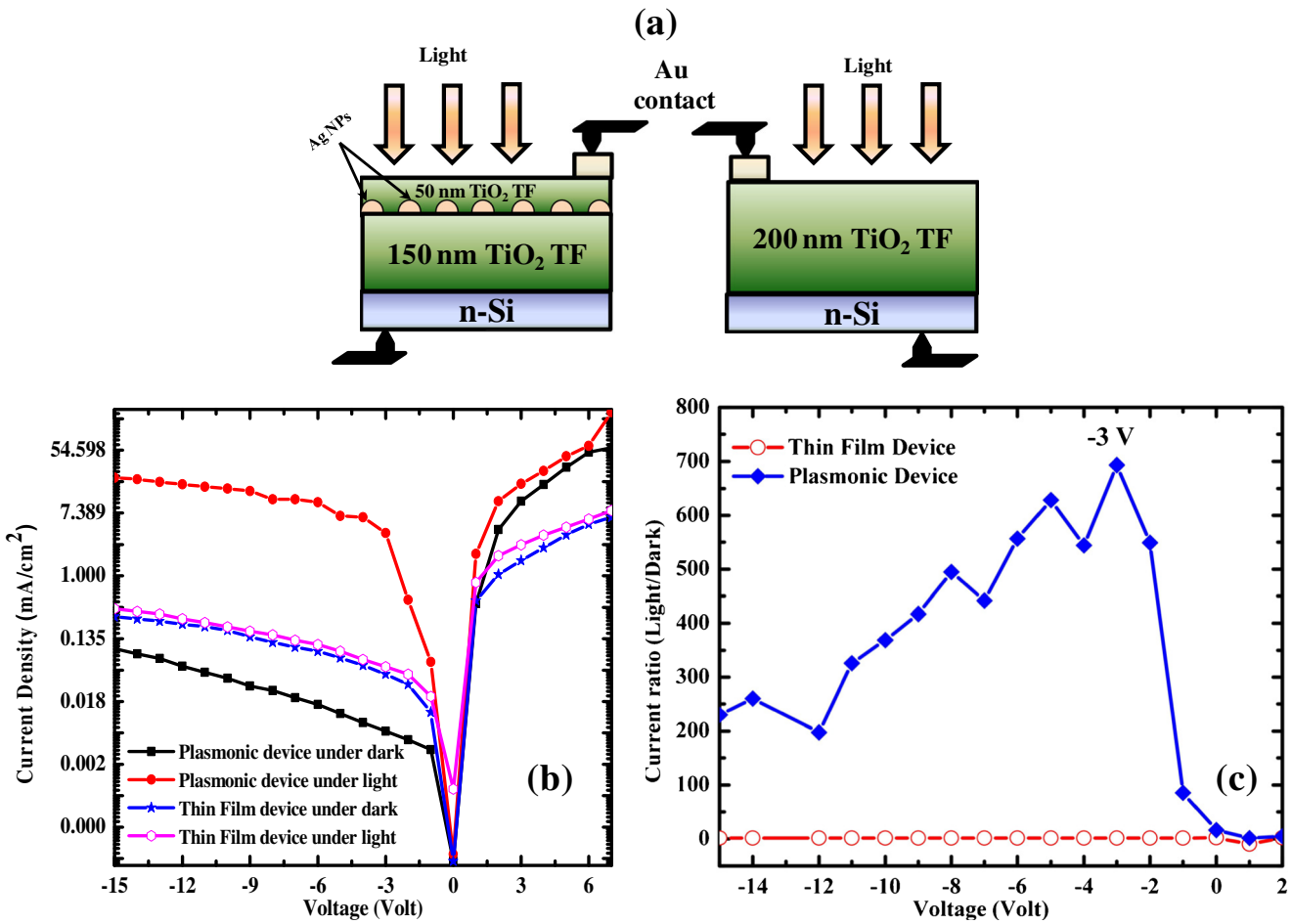

Fig. 1 **a** The schematic of Ag NPs-patterned TiO_2 TF (plasmonic) and the bare TiO_2 TF-based devices. **b** I–V characteristics of TiO_2 TF device and Ag NPs/TiO_2 TF plasmonic device through Au Schottky contact. **c** Light/dark current of the plasmonic and thin film devices through Au contact

Where, A^{**} (9.4 A cm^{-2} K^{-2}) [19] is the effective Richardson constant and φ_b is the barrier height at zero bias. The barrier height can be obtained from the equation

$$\phi_b = \frac{kT}{q}\ln\left(\frac{AA^{**}T^2}{I_0}\right) \tag{4}$$

Using the thermionic emission (TE) model, the Schottky barrier height (SBH) (φ_b) and ideality factor (n) of the devices were determined from log I–V (Fig. 1b) characteristic. The calculated value of ϕ_b from the I–V characteristics of TiO_2 TF and Ag NPs/TiO_2 TF-based plasmonic device under dark condition were 0.36 and 0.43 eV, respectively. The ideality factor n is defined as

$$n = \frac{q}{kT}\frac{dV}{d(\ln(I))} \tag{5}$$

The ideality factor n can be determined from the slope of linear region of semi-log forward I–V plots (Fig. 1b) using the above equation. The ideality factor of plasmonic device was found to be ~9.5 (calculated from Fig. 1b) and for thin film device was ~8 (calculated from Fig. 1b). Our results showed that the ideality factors of Au/TiO_2 Schottky contacts were higher than the unity. For an ideal diode, the diode ideality factor n should be nearly equal to unity. A high ideality factor is often attributed to defect states in the semiconductor band gap [20]. In a real situation, it may increase due to the effects of series resistance, leakage current, in-homogeneities of film thickness, and presence of interface states at the junction of the diode. The presence of interface defect states at the junction or metal–semiconductor junction is responsible for tunneling process. Therefore, the current conduction in such cases is dominated by tunneling instead of diffusion, which enhances the ideality factor of the detector. In our case, the deposition of Ag NPs on TiO_2 TF introduced more oxygen-related defects [7], which appeared at the interface of Au/TiO_2 TF. The presence of these defects could be responsible for high tunneling process in the plasmonic device and the increase in the value of ideality factor as compared to TiO_2 TF detector.

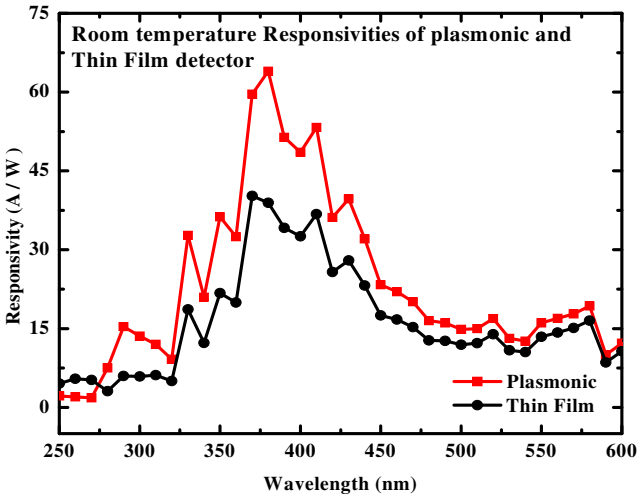

Fig. 2 Photo responsivities of the devices

High Internal Gain

Figure 2 shows the device responsivity measured at different wavelengths under the applied reverse bias of −3 V. The maximum internal gain for the device was calculated to be ~210 at UV region (380 nm) by using the following relation [21],

$$G = \frac{R \times h \times c}{\lambda \times e \times \eta} \tag{6}$$

Where R is the responsivity of the device, h is the Planck's constant, c is the speed of light, λ is the wavelength of incident radiation, e is the electronic charge, and η is the quantum efficiency (assuming η=1). The internal gain was found to be much higher than those reported by Zhang et al. for TiO_2 (~142.3) [22] and $Zr_{0.5}Ti_{0.5}O_2$ based solar blind ultraviolet photo detector (~3.1) [23].

The high internal gain of the AgNPs/TiO_2 TF/ n-Si-based plasmonic detector was due to enhanced photon absorption and presence of oxygen defect related more trap states into the band gap of TiO_2 material and their corresponding conduction as discussed earlier.

Junction Capacitance of the Device

The junction capacitances of the detectors were measured to determine the contribution of the trap states in device operation. The junction capacitance of the TiO_2 TF/n-Si and TiO_2 TF/Ag NPs/TiO_2 TF/n-Si (plasmonic)-based devices were measured through Ag Schottky contact using LCR meter (Agilent E4980-A). Figure 3 shows the capacitance (C)–voltage (V) curves at different frequencies both for the TiO_2 TF (Fig. 3a) and Ag NPs/TiO_2 TF (Fig. 3b)-based devices. The variations of capacitance were highlighted for the inversion region of the devices.

The capacitance of the TiO_2 TF-based device decreased from ~87 to ~6 pF and for Ag NPs/TiO_2 TF-based plasmonic device from ~57 to ~4 pF due to the increase in frequency from 100 KHz to that of 2 MHz, measured at −12 V applied potential at the top Ag contact. A large amount of variation in inversion capacitance ~81 pF was calculated for the TiO_2 TF-based device, which was larger than that of the plasmonic device ~53 pF. The presence of trap states at the interface of Ag/TiO_2 responded efficiently at lower frequencies, which resulted in the anomalous behavior of the junction capacitance of the devices. Therefore, the small numbers of traps into TiO_2 TF were incapable to follow the a.c. signal at higher frequency estimated to the case of Ag NPs/TiO_2 TF-based plasmonic detector. The mechanism of following the a.c. signals by the trap states present in TiO_2 nanowires (NWs)-based devices and its anomalous C–V behavior were described by the authors [24, 25]. A moderate variation ~53 pF of inversion capacitance for plasmonic-based device compared to TiO_2

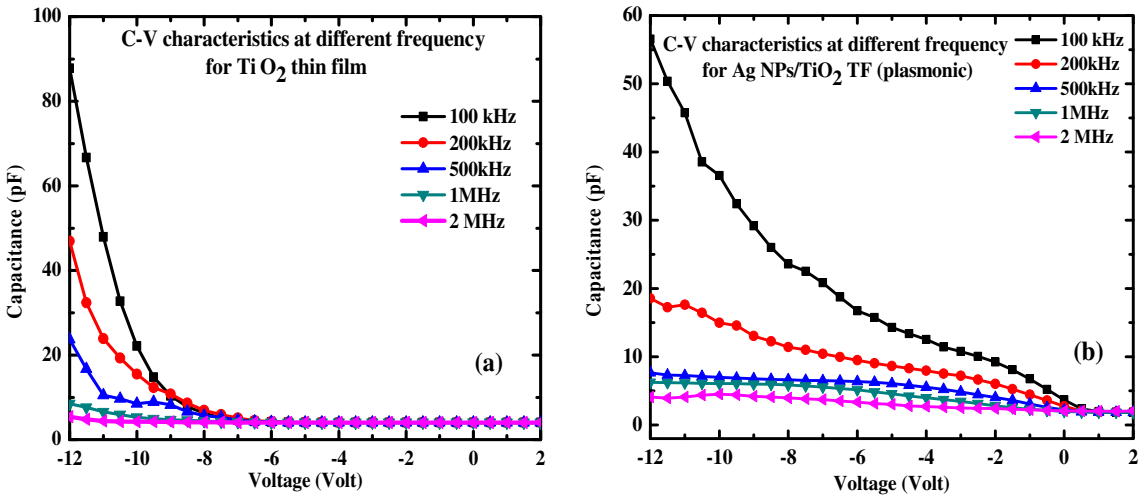

Fig. 3 Frequency-dependent C–V characteristics for **a** TiO_2 TF and **b** Ag NPs/TiO_2 TF (plasmonic) devices

TF device may be due to the efficient response of traps at higher frequency.

Memory Window

The capacitance–voltage characteristics (Fig. 4a, b) of the TiO_2 TF and plasmonic devices were measured separately at 1 MHz to find out the charge-trapping into the devices. The memory windows of the devices were calculated from the C–V curves in the inversion region.

The change of capacitance with respect to the applied voltage on the devices are shown for TiO_2 TF (Fig. 4a) and Ag NPs/TiO_2 TF (Fig. 4b) under a sweeping top electrode voltage from ±6 to ±10 V. Figure 4c displayed the memory windows for different sweeping top electrode voltage. A memory window of $\Delta V \approx 0.63$ V for TiO_2 TF and $\Delta V \approx 0.52$ V for plasmonic devices were calculated under a sweeping top electrode voltage (V_s) from +6 to −6 V, and then back to +6 V. The memory window increases with the increase of the sweeping top electrode voltages. When the applied sweeping top electrode voltages Vs were ±8 and ±10 V, the corresponding maximum memory windows in its C–V curves were about 1.8 and 2.1 V for TiO_2 TF and about 1.9 and 4.5 V for plasmonic devices. Lee et al. have reported that the presence of Pt NPs into TiO_2 TF can induce charge trap states [11]. In our case, the presence of Ag NPs into the TiO_2 TF matrix acted as charge trap elements, which resulted to large memory window for the plasmonic device compared to bare TiO_2 TF.

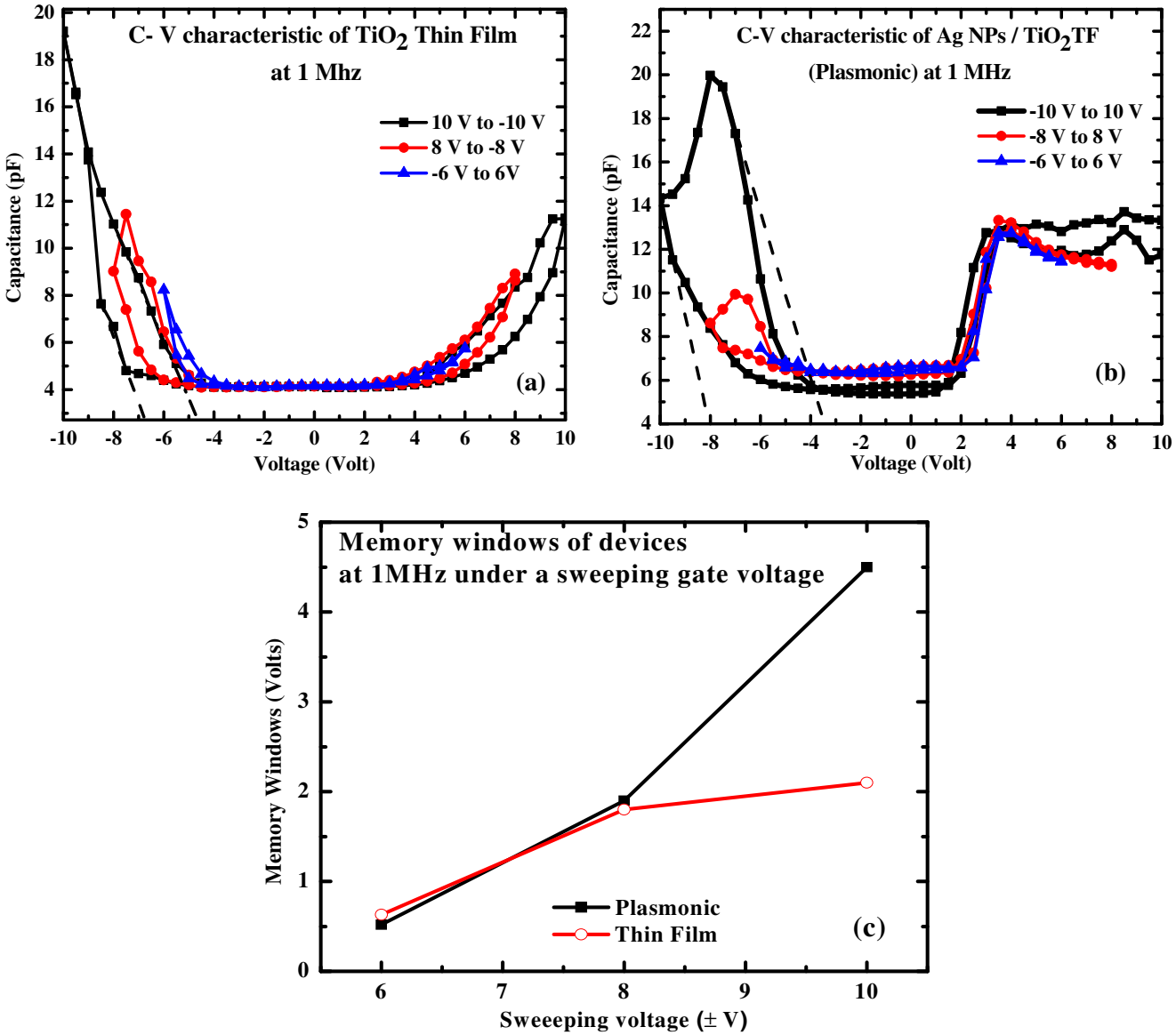

Fig. 4 C–V curves at 1 MHz under a sweeping top electrode voltage from ±6 to ±10 V for **a** TiO_2 TF and **b** Ag NPs/TiO_2 TF devices. **c** Memory windows of the devices

Device Impedance

Figure 5a, b displayed the frequency dependent impedance at different applied potential from −7 to +12 V, for both TiO_2 TF and Ag NPs/TiO_2 TF-based devices. The maximum impedance of 720 KΩ was recorded for the Ag NPs/TiO_2 TF-based device at 100 KHz, which decreased to 35 KΩ at 2 MHz. In case of bare TiO_2 TF, the low impedance of 384 KΩ (100 KHz) and 20 KΩ (2 MHz) was observed as compared to Ag NPs/TiO_2 TF-based device. Due to the introduction of Ag NPs into the TiO_2 matrix, the oxygen-related defect states were increased (described in the above sections), which enhanced the trap states at the metal semiconductor interface.

The presence of trap states into the material held the electrons and decreased the mobility of the device and therefore showed the high impedance of the Ag NPs/TiO_2 TF device. The experiment reversely supported the reason of getting low dark current from the TiO_2 TF/Ag NPs/TiO_2 TF/n-Si (plasmonic) based device as compared to TiO_2 TF/n-Si (shown in Fig. 1b) using Au Schottky contact. Therefore, we have observed the same role of trap states in device operation, both for the cases of Ag and Au top electrodes. Finally, it can be manifested that the introduction of defect states due to the presence of Ag NPs into TiO_2 band gap, assisted large photon absorption and therefore the photoconduction. Again, the presence of trap states reduced the dark conductivity and charge-trapping capability of the plasmonic device, which can be proposed for the fabrication of nonvolatile memory devices. The enhanced photoconduction suggested that the Ag NPs/TiO_2 TF system is capable for efficient photo energy conversion.

Conclusion

The enlarged photocurrent under photon illumination of the Ag NPs/TiO_2 TF (plasmonic) device was observed at reverse bias condition than that at forward bias. Under xenon lamp excitation, with top Au electrode the plasmonic device produced maximum ~700 times enlarged current at applied voltage −3 V, due to coupling of Ag NPs LSPRs and TiO_2 medium together with the hole trapping process. A large ideality factor of 9.5 was calculated for the plasmonic device as compared with 8 for bare TiO_2 TF. The presence of large numbers of oxygen-related defect states at the interface of metal and semiconductor induced tunnel current into the device, which increased the ideality factor. The maximum internal gain of ~210 was calculated for the plasmonic detector in the UV region at 380 nm. The capacitances of the TiO_2 TF and Ag NPs/TiO_2 TF-based plasmonic devices were measured with different biasing voltages under the variation of frequency from 200 KHz to that of the 2 MHz. The continuous decrease in inversion capacitance with increase in frequency was observed with moderate variation (~53 pF) in case of plasmonic device as compared to TiO_2 TF (~81 pF), which might be due to the presence of huge numbers of traps in plasmonic devices. The maximum memory window of 4.5 V was determined for the Ag NPs/TiO_2 TF-based device as compared to bare TiO_2 TF of 2.1 V under sweeping top electrode voltage of ±10 V. The presence of high memory window in case of Ag NPs/TiO_2 TF was due to the large trap densities and corresponding charge trapping. Due to the introduction of Ag NPs into the TiO_2 matrix, the oxygen-related defect states were increased, which enhanced the trap states at the metal semiconductor interface and the impedance of the Ag NPs/TiO_2 TF device. Finally, the presence of memory window suggests that the plasmonic devices also can be used

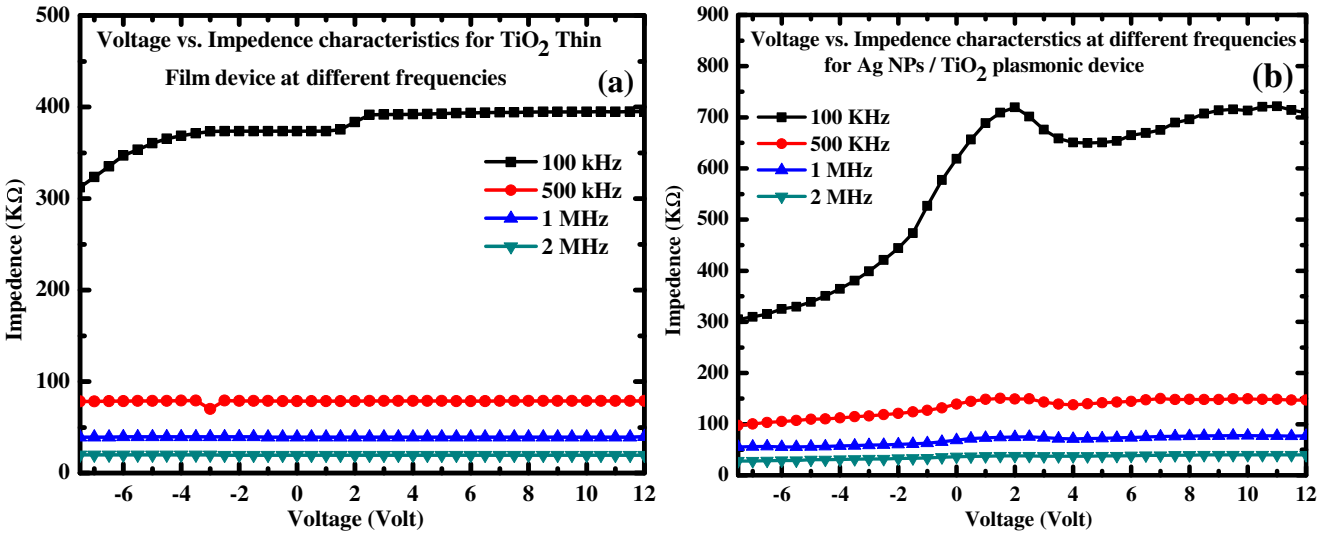

Fig. 5 Frequency dependent impedance for **a** TiO_2 TF and **b** Ag NPs/TiO_2 TF-based plasmonic devices

as charge-trapping memory device and large photoconduction property for efficient energy harvesting.

Acknowledgments The authors are grateful to the Department of Science and Technology, Govt. of India, TEQIP-II, and National Institute of Technology Agartala for financial support.

References

1. Fujishima A, Honda K (1972) Electrochemical photolysis of water at a semiconductor electrode. Nature 238:37–38
2. Linsebigler L, Lu G, Yates JT (1995) Photocatalysis on TiO_2 surfaces: principles, mechanisms, and selected results. Chem Rev 95: 735–758
3. Nakata K, Ochiai T, Murakami T, Fujishima A (2012) Photoenergy conversion with TiO_2 photocatalysis: new materials and recent applications. Electrochim Acta 84:103–111
4. Yin WJ, Chen S, Yang JH, Gong XG, Yan Y, Wei SH (2010) Effective band gap narrowing of anatase TiO_2 by strain along a soft crystal direction. Appl Phys Lett 96:221901-1–221901-3
5. Awazu K, Fujimaki M, Rockstuhl C, Tominaga J, Murakami H, Ohki Y, Yoshida N, Watanabe T (2008) A plasmonic photocatalyst ponsisting of silver nanoparticles embedded in titanium dioxide. J Am Chem Soc 130:1676–1680
6. Tofflinger JA, Pedrueza E, Chirvony V, Leendertz C, Calzada RG, Abargues R, Gref O, Roczen M, Korte L, Pastor JPM, Rech B (2013) Photoconductivity and optical properties of silicon coated by thin TiO_2 film in situ doped by Au nanoparticles. Phys Status Solidi A 210:687–694
7. Ganguly A, Mondal A, Dhar JC, Singh NK, Choudhury S (2013) Enhanced visible light absorption by TiO_2 film patterned with Ag nanoparticles arrays. Phys E 54:326–330
8. Mondal A, Singh NK, Chinnamuthu P, Dhar JC, Bhattacharyya A, Choudhury S (2012) Enlarged photodetection using SiO_x nanowire arrays. IEEE Photon Tech L 24(22):2020–2023
9. Lee C, Kim I, Shin H, Kim S, Cho J (2010) Nonvolatile memory properties of Pt nanoparticle-embedded TiO_2 nanocomposite multilayers via electrostatic layer-by-layer assembly. Nanotechnology 21: 185704-1–185704-7
10. Lan X, Ou X, Cao Y, Tang S, Gong C, Xu B, Xia Y, Yin J, Li A, Yan F, Liu Z (2013) The effect of thermal treatment induced interdiffusion at the interfaces on the charge trapping performance of HfO_2/Al_2O_3 nanolaminate-based memory devices. J. Appl. Phys. 114: 044104 - 044104–7
11. Spiga S, Driussi F, Lamperti A, Congedo G, Salicio O (2012) Effects of thermal treatments on the trapping properties of HfO_2 films for charge trap memories. Appl Phys Express 5: 021102-1–021102-3
12. Lan X, Ou X, Lei Y, Gong C, Liu Z (2013) The interface interdiffusion induced enhancement of the charge-trapping capability in HfO_2/Al_2O_3 multilayered memory devices .Appl. Phys. Lett. 103: 192905 - 192905–5
13. Choudhuri B, Mondal A, Dhar J C, Singh NK, Goswami T, Chattopadhyay KK (2014) Enhanced photocurrent from generated photothermal heat in indium nanoparticles embedded TiO_2 film. Appl. Phys. Lett. 102 (23): 233108 - 233108–4
14. Ganguly A, Mondal A, Choudhuri B, Goswami T, Chattopadhyay KK (2014) Ag nanoparticles patterned TiO_2 thin film plasmonic detector for enlarged light detection. Adv Sci Eng Med 6:797–801
15. Chinnamuthu P, Mondal A, Singh NK, Dhar JC, Chattopadhyay KK, Bhattacharya S (2012) Band gap enhancement of glancing angle deposited TiO_2 nanowire array. J. Appl. Phys. 112 : 054315 - 054315–6
16. Das SN, Kar JP, Myoung JM (2011) Nanowires fundamental research. InTech Publishing, Rijeka, p 174
17. Das SN, Moon KJ, Kar JP, Choi JH, Xiang (2010) ZnO single nanowire-based UV detectors. J Appl. Phys, lett. 97: 022103 - 022103–3
18. Sze SM, Ng KK (2008) Physics of semiconductor devices. John Wiley & Sons, New Jersey, p 154
19. Williams RH, Robinson GY (1985) Physics and chemistry of III–V compound semiconductor interfaces. Plenum Press, New York, p 86
20. Werner JH, Guttler HH (1991) Barrier inhomogeneities at Schottky contacts. J Appl Phys 69:1522–1533
21. Nayfeh OM, Rao S, Smith A, Therrien J, Nayfeh MH (2004) Thin film silicon nanoparticle UV photodetector. IEEE Photon Tech L 16: 1927–1929
22. Zhang M, Zhang H, Kaibo L, Chen W, Zhou J, Shen L, Ruan S (2012) Ultraviolet photodetector with high internal gain enhanced by $TiO_2/SrTiO_3$ heterojunction. Opt Express 20: 5936–5941
23. Zhang M, Gu X, Kaibo L, Dong W, Ruan S, Chen Y, Zhang H (2013) High response solar-blind ultraviolet photodetector based on $Zr_{0.5}Ti_{0.5}O_2$ film. Appl Surf Sci 268:312–316
24. Mondal A, Dhar JC, Chinnamuthu P, Singh NK, Chattopadhyay KK, Das SK, Das SC, Bhattacharyya A (2013) Electrical properties of vertically oriented TiO_2 nanowire arrays synthesized by glancing angle deposition technique. Electron Mater Lett 9(2):213–217
25. Dhar JC, Mondal A, Chinnamuthu P, Singh NK (2013) Low leakage TiO_2 nanowire dielectric MOS device using Ag Schottky gate contact. IEEE T Nanotechnol 12:948–950